J. Fluid Mech. (1973), *vol.* 58, *part* 2, *pp.* 289–312
Printed in Great Britain

Two-dimensional Rayleigh–Bénard convection

By D. R. MOORE AND N. O. WEISS

Department of Applied Mathematics and Theoretical Physics,
University of Cambridge

(Received 7 July 1972 and in revised form 1 December 1972)

Two-dimensional convection in a Boussinesq fluid confined between free boundaries is studied in a series of numerical experiments. Earlier calculations by Fromm and Veronis were limited to a maximum Rayleigh number R 50 times the critical value R_c for linear instability. This range is extended to $1000R_c$. Convection in water, with a Prandtl number $p = 6{\cdot}8$, is systematically investigated, together with other models for Prandtl numbers between 0·01 and infinity. Two different modes of nonlinear behaviour are distinguished. For Prandtl numbers greater than unity there is a viscous regime in which the Nusselt number $N \approx 2(R/R_c)^{\frac{1}{2}}$, independently of p. The heat flux is a maximum for cells whose width is between 1·2 and 1·4 times the layer depth. This regime is found when $5 \leqslant R/R_c \lesssim p^{\frac{3}{2}}$. At higher Rayleigh numbers advection of vorticity becomes important and $N \propto R^{0{\cdot}365}$. When $p = 6{\cdot}8$ the heat flux is a maximum for square cells; steady convection is impossible for wider cells and finite amplitude oscillations appear instead, with periodic fluctuations of temperature and velocity in the layer. For $p < 1$ it is also found that $N \propto R^{0{\cdot}365}$, with a constant of proportionality equal to 1·90 when $p \ll 1$ and decreasing slowly as p is increased. The physical behaviour in these regimes is analysed and related to astrophysical convection.

1. Introduction

The characteristic features of astrophysical convection are not easily reproduced in the laboratory. They can, however, be investigated through numerical experiments, and more physical understanding may be gained from studying a planned sequence of idealized models than from attempting to describe every detail of a star's convective zone. The simplest relevant problem, that of convection in a Boussinesq fluid, confined between slippery horizontal planes and heated from below, was first defined by Rayleigh (1916) and has been treated by many others since (Chandrasekhar 1961; Brindley 1967; Spiegel 1971*b*). For computation it is convenient to restrict the flow to two dimensions and this idealized form of Rayleigh–Bénard convection was investigated by Fromm (1965) and Veronis (1966). We first looked at this problem in order to check a general program for two-dimensional convection and assess the limitations of our numerical approximation by comparison with published results. To our surprise we found that the subject had not yet been exhausted.

Steady convection can be described by expressing the Nusselt number N as

a function of the Prandtl number p and the ratio of the Rayleigh number R to its critical value R_c for linear instability. This new investigation helps to provide a physical understanding of two-dimensional convection between free boundaries for the range $p \geqslant 0{\cdot}01$ and $R \leqslant 1000\,R_c$, limited by the computer time available. The maximum Rayleigh number reliably examined has been extended from Fromm's limit of $18{\cdot}5R_c$ and Veronis' of $50R_c$ to a value of $1000R_c$. This has clarified the existence of two distinct regimes, with different dependence of N on R. A one-third power law was found by Herring (1963), using the mean field approximation (Spiegel 1967), and by Fromm; it is implicit also in the work of Veronis. For *viscous* convection (when advection of vorticity is negligible) we have confirmed that

$$N \approx 2(R/R_c)^{\frac{1}{3}}, \tag{1}$$

and is independent of p, but this holds only for $5 \leqslant R/R_c \lesssim p^{\frac{3}{2}}$. At high Reynolds numbers, when *advection* dominates diffusion of vorticity,

$$N \approx A(p)\,(R/R_c)^{0{\cdot}365}, \tag{2}$$

where $A(p) \approx 1{\cdot}95p^{-0{\cdot}05}$ for $p \geqslant 6{\cdot}8$ and tends to a limit of $1{\cdot}90$ as $p \to 0$.

Steady two-dimensional convection can be found at any Rayleigh number for suitably chosen cell widths; its nature is determined by the balance between advection and diffusion of vorticity. It has sometimes been conjectured that two-dimensional rectangular cells must always settle down to a steady state. However, we have found that time-dependent behaviour persists in flattened cells for $p > 1$, $R \geqslant 100R_c$. The coupling between temperature and velocity maintains periodic finite amplitude oscillations, as in Welander's (1967) simple model.

In the next section we formulate the mathematical system to be solved and express the equations in dimensionless form. The numerical techniques are then described in order to discuss the accuracy of results obtained on a given mesh. It was necessary to develop finite-difference methods on a rectangular grid so as to resolve boundary layers at high Rayleigh numbers. The results of the numerical experiments are presented and discussed in § 4. Their physical interpretation is considered in the following section. (Note that the results in § 4 are given in dimensionless units though the discussion of § 5 uses physical, dimensional quantities.) Finally, we indicate how the work might be extended and relate it to other, more complicated problems.

2. Formulation of the problem

In a Boussinesq fluid the velocity $\mathbf{u}$ satisfies the Navier–Stokes equation

$$\rho_0\left[\frac{\partial \mathbf{u}}{\partial t} + (\mathbf{u}.\nabla)\,\mathbf{u}\right] = -\nabla P + \rho\mathbf{g} + \rho_0\nu\nabla^2\mathbf{u} \tag{3}$$

and the incompressibility condition

$$\nabla.\mathbf{u} = 0, \tag{4}$$

where P is the pressure, $\mathbf{g}$ the gravitational acceleration and ν the kinematic viscosity; the equation of state is

$$\rho(T) = \rho_0[1-\alpha(T-T_0)], \tag{5}$$

where the density ρ has the value ρ_0 when the temperature T is equal to T_0 and α is the coefficient of thermal expansion. Pressure can be eliminated by taking the curl of (3); then

$$\partial\boldsymbol{\omega}/\partial t = \nabla \wedge (\mathbf{u} \wedge \boldsymbol{\omega}) - \alpha\nabla T \wedge \mathbf{g} + \nu\nabla^2\boldsymbol{\omega}, \tag{6}$$

where the vorticity $\boldsymbol{\omega} = \nabla \wedge \mathbf{u}$. Finally, the heat flow equation gives

$$\partial T/\partial t = -\nabla.(T\mathbf{u}) + \kappa\nabla^2 T, \tag{7}$$

where κ is the thermometric conductivity.

For two-dimensional convection we choose Cartesian axes with z vertical so that all flow is confined to the x, z plane and independent of y. Then

$$\mathbf{u} = (u, 0, w), \quad \boldsymbol{\omega} = (0, \omega, 0), \tag{8}$$

while, from (4), there exists a stream function ψ such that

$$u = -\partial\psi/\partial z, \quad w = \partial\psi/\partial x, \quad \omega = -\nabla^2\psi. \tag{9}$$

Equation (6) then simplifies to

$$\frac{\partial\omega}{\partial t} = -\nabla.(\omega\mathbf{u}) - g\alpha\frac{\partial T}{\partial x} + \nu\nabla^2\omega, \tag{10}$$

which, apart from the buoyancy term, is similar to (7).

We restrict the calculation to the rectangular region $0 \leqslant x \leqslant L$, $0 \leqslant z \leqslant d$ and adopt the following boundary conditions.

(i) On $z = 0$, d the normal velocity and tangential stress both vanish, while the temperatures are fixed: hence

$$\psi = 0, \quad \omega = 0 \quad (z = 0, d) \tag{11}$$

and

$$T = T_0 \quad (z = d), \qquad T = T_0 + \Delta T \quad (z = 0). \tag{12}$$

(ii) The stream function is assumed to be an odd function of x and periodic, with period $2L$, so that

$$\psi = 0, \quad \omega = 0, \quad \partial T/\partial x = 0 \quad (x = 0, L). \tag{13}$$

In the absence of convection there would be a uniform vertical temperature gradient and a thermometric flux $F_0 = \kappa\Delta T/d$. When convection occurs, the horizontally averaged thermometric flux is

$$F = \overline{wT - \kappa\,\partial T/\partial z} \tag{14}$$

and the normalized flux is given by their ratio, the Nusselt number

$$N = \frac{F}{F_0} = \frac{d}{\Delta T}\left[\frac{1}{\kappa}\overline{wT} - \frac{d\bar{T}}{dz}\right]. \tag{15}$$

It is usual to express the equations in dimensionless form. We find it convenient to use a time unit based on the buoyancy force (analogous to the Brunt–Väisälä period) so that the dimensionless (primed) quantities become

$$(x', z') = d^{-1}(x, z), \quad t' = \left(\frac{g\alpha\Delta T}{d}\right)^{\frac{1}{2}} t, \quad T' = \frac{T - T_0}{\Delta T}. \tag{16}$$

In terms of the Rayleigh number

$$R = g\alpha\Delta T d^3/\kappa\nu \tag{17}$$

and the Prandtl number

$$p = \nu/\kappa, \tag{18}$$

the dimensionless velocity, conductivity and viscosity are then

$$\mathbf{u}' = (pR)^{-\frac{1}{2}} d\kappa^{-1}\mathbf{u}, \quad \kappa' = (pR)^{-\frac{1}{2}}, \quad \nu' = (p/R)^{\frac{1}{2}}. \tag{19}$$

Finally, suppressing primes, we can rewrite (7), (10) and (9) in the form

$$\partial T/\partial t = -\nabla.(T\mathbf{u}) + \kappa\nabla^2 T, \tag{20}$$

$$\frac{\partial\omega}{\partial t} = -\nabla.(\omega\mathbf{u}) - \frac{\partial T}{\partial x} + \nu\nabla^2\omega \tag{21}$$

and

$$\nabla^2\psi = -\omega. \tag{22}$$

Equations (20), (21) and (22) have to be solved in the region $0 \leqslant x \leqslant \lambda$, $0 < z < 1$, where the normalized cell width

$$\lambda = L/d, \tag{23}$$

subject to boundary conditions

$$T = 1 \quad (z = 0), \qquad T = 0 \quad (z = 1), \qquad \partial T/\partial x = 0 \quad (x = 0, \lambda) \tag{24}$$

and

$$\omega = 0, \quad \psi = 0 \quad (x = 0, \lambda; z = 0, 1). \tag{25}$$

The effectiveness of convection is now measured by a Nusselt number

$$N = \frac{1}{\kappa}\overline{wT} - \frac{d\overline{T}}{dz}, \tag{26}$$

while the vigour of the motion is indicated by the average, dimensionless kinetic energy density

$$\mathscr{E} = \frac{1}{2\lambda}\int_0^1\int_0^\lambda \omega\psi\, dx\, dz. \tag{27}$$

The boundary conditions (24) and (25) already imply that the partial differential equations (20)–(22) need only be solved over half of the full convection cell with $0 \leqslant x \leqslant 2\lambda$; the solutions show mirror symmetry about the planes $x = 0$, $x = \lambda$. We can also take advantage of a further symmetry property: symmetry of ψ and T about the midpoint $x = \frac{1}{2}\lambda$, $z = \frac{1}{2}$, such that

$$\psi(x, z) = \psi(\lambda - x, 1 - z) \tag{28}$$

and

$$T(x, z) + T(\lambda - x, 1 - z) = 1 \tag{29}$$

is preserved by the equations. This can be verified by Fourier analysis (Veronis 1966). Thus the equations have to be solved only over the quarter-cell $0 \leqslant x \leqslant \lambda$,

$0 < z \leqslant \frac{1}{2}$, with appropriate boundary conditions on $z = \frac{1}{2}$. This simplification is particularly convenient for computation.

Our boundary conditions allow no horizontal velocity at $x = 0$. Greater generality could be achieved by letting ψ be periodic in x without insisting that $\psi(0, z) = 0$. This would permit lateral sloshing (Deardorff & Willis 1965) and also allow the development of cells with widths λ/m, where m is any integer. We have preferred to impose more stringent boundary conditions so as to facilitate investigations at high Rayleigh numbers. Thus (24) and (25) inhibit the transition from a configuration with odd m to cells with m even (and vice versa). The conditions (28) and (29) are even stronger and prohibit the growth of cells unless m is odd. It is easy to find particular cases where the solution may depend upon the boundary conditions that have been adopted, but the overall behaviour of convection is generally unaffected.

3. Numerical methods

The nonlinear partial differential equations (20)–(22) were solved by finite-difference methods; these will be described in detail elsewhere (Moore, Peckover & Weiss 1973) and need only be summarized here. The variables T, ω and ψ are represented on a rectangular grid with spacing Δx, Δz; let $x_j = j\Delta x$, $z_k = k\Delta z$ and $t^n = n\Delta t$, where $j = 0, 1, \ldots, N_x$ and $k = 0, 1, \ldots, N_z$, and put $T^n_{j,k} = T(x_j, z_k; t^n)$ etc. Equations (20) and (21) are advanced by a second-order leapfrog scheme, centred in time and space (Roberts & Weiss 1966). With $\Delta x = \Delta z$, equation (21) becomes

$$\begin{aligned}\omega^{n+1}_{j,k} = \omega^n_{j,k} + \frac{\Delta t}{4(\Delta z^2 + 2\nu\Delta t)} [&(\psi^{n+\frac{1}{2}}_{j+1,k+1} - \psi^{n+\frac{1}{2}}_{j+1,k-1})\,\omega^{n+\frac{1}{2}}_{j+1,k} \\ &- (\psi^{n+\frac{1}{2}}_{j-1,k+1} - \psi^{n+\frac{1}{2}}_{j-1,k-1})\,\omega^{n+\frac{1}{2}}_{j-1,k} - (\psi^{n+\frac{1}{2}}_{j+1,k+1} - \psi^{n+\frac{1}{2}}_{j-1,k+1})\,\omega^{n+\frac{1}{2}}_{j,k+1} \\ &+ (\psi^{n+\frac{1}{2}}_{j+1,k-1} - \psi^{n+\frac{1}{2}}_{j-1,k-1})\,\omega^{n+\frac{1}{2}}_{j,k-1} - 2\Delta z(T^{n+\frac{1}{2}}_{j+1,k} - T^{n+\frac{1}{2}}_{j-1,k}) \\ &+ 4\nu(\omega^{n+\frac{1}{2}}_{j+1,k} + \omega^{n+\frac{1}{2}}_{j-1,k} + \omega^{n+\frac{1}{2}}_{j,k+1} + \omega^{n+\frac{1}{2}}_{j,k-1} - 4\omega^n_{j,k})]. \end{aligned} \tag{30}$$

This, with a similar equation for $T^{n+1}_{j,k}$, is solved explicitly for all points with $j + k$ even, while values of ω and T at points with $j + k$ odd are subsequently calculated at $t^{n+\frac{3}{2}}$. The stream function ψ is obtained by solving Poisson's equation in the form

$$\psi_{j+1,k+1} + \psi_{j+1,k-1} + \psi_{j-1,k+1} + \psi_{j-1,k-1} - 4\psi_{j,k} = -2\Delta z^2 \omega_{j,k}, \tag{31}$$

using fast Fourier analysis in the x direction and tridiagonal elimination in the z direction. Unfortunately, (31) gives ψ at the same points as ω, which is not what is wanted for (30), so the required values must be obtained by fourth-order interpolation from the formula

$$\begin{aligned}\psi_{j,k} = \tfrac{1}{4}[&(\psi_{j+1,k} + \psi_{j-1,k} + \psi_{j,k+1} + \psi_{j,k-1}) \\ &+ \tfrac{1}{4}\Delta z^2(\omega_{j+1,k} + \omega_{j-1,k} + \omega_{j,k+1} + \omega_{j,k-1})]. \end{aligned} \tag{32}$$

This method was applied over an entire half-cell ($0 < x \leqslant \lambda$, $0 < z < d$), with a maximum of 48 intervals in the range $0 \leqslant x \leqslant \lambda$. The boundary values at $z = 0, 1$ remain unaltered throughout the calculation and the temperatures at $x = 0, \lambda$ are easily computed.

It is essential to establish the accuracy of any difference scheme and, for convection problems, the maximum Rayleigh number that can be studied on a given mesh. At high Rayleigh numbers the temperature variation is concentrated into narrow boundary layers (see figure 6) of thickness $\delta \approx (2N)^{-1}$. To resolve such a layer adequately it is necessary to have at least three intervals across it (cf. the discussion of convection with fixed boundaries by Schneck & Veronis 1967). Hence we need to have $N_z > 6N$; conversely, for a mesh with fixed N_z we are, from (1), restricted to Rayleigh numbers such that

$$R/R_c \leqslant (\tfrac{1}{12}N_z)^3. \tag{33}$$

For example, a model computed with 18 intervals is accurate only for $N \leqslant 3$ or $R/R_c \leqslant 4$; with $N_z = 34$, we need $N \leqslant 6$ and $R/R_c \leqslant 25$. Comparison of actual results (see table 1 below) confirms that this is a correct, if somewhat cautious, criterion: for $N_z = 18$ the error in the Nusselt number rises from 1 % at $N = 3$ to 2 % at $N = 6$, though a global quantity like N may provide an over-optimistic measure of accuracy.

The horizontal length scale associated with variations of temperature and vorticity is greater than the vertical. So it is possible to use a grid with $\Delta x > \Delta z$, and appropriate difference schemes were therefore developed in order to resolve the thermal boundary layers at high Rayleigh numbers. The modifications to (30) and (32) when $\Delta x \neq \Delta z$ are straightforward but the left-hand side of (31) has to be replaced by a seven-point representation of the Laplacian, requiring pentadiagonal elimination in the z direction. This version was implemented over the quarter-cell $0 \leqslant x \leqslant \lambda$, $0 < z \leqslant \frac{1}{2}$, with $\Delta x > \Delta z$ (Moore *et al.* 1973). The mesh only covers half the layer depth, so $N_z = (2\Delta z)^{-1}$ and values of ψ_{j,N_z+1} etc. are derived from (28) and (29). This procedure halves the number of points used and runs were made with $\Delta z \gtrsim \frac{1}{4}\Delta x$ on meshes with up to 48×100 points (the largest practicable on the machine). The correctness of the method was checked by comparison with cases run using both half-cells and the full cell, $0 \leqslant x \leqslant 2\lambda$, $0 < z < 1$.

For $R \leqslant 200R_c$ the vertical plumes were adequately described with $N_x = 24$; this was confirmed by cases run with $N_x = 48$. The width of the cell could be set to any desired values and the number of vertical intervals chosen to resolve the structure at the expected Nusselt number. There is only one boundary layer in the quarter-cell and we allowed four intervals across it, giving $N_z \approx 4N$. The adequacy of this approximation was again confirmed by comparison with cases run with $N_z = 8N$. With 48 intervals horizontally and 100 vertically, Nusselt numbers up to 25 could be examined; this corresponds to $R \approx 1700R_c \approx 10^6$. In fact, limited computer time restricted our investigation to $R = 1000R_c$; this case was run for 4000 times steps, and took 5 h of computing time on an IBM 360/44.

The various arrays were monitored during each run, and two averaged quantities, the Nusselt number and the kinetic energy density, were calculated from approximations to (26) and (27). The Nusselt number was evaluated in the middle of each vertical interval by calculating the average temperature gradient and the mean of the convected heat fluxes at the two adjacent levels. The alternative procedure, of averaging the gradient vertically, is less accurate.

For $R < 40R_c$, cases were run until N converged to the limit set by machine accuracy (1 in 10^7); the Nusselt number was constant from level to level to one part in 10^4. For $R > 40R_c$ the solutions oscillated and some cases did not converge to steady states. The oscillations in converging cases were quite distinct from those that persisted at a constant amplitude. The former were computed until their amplitude had fallen by at least a factor of $1/e$ (typically 4–8 cycles). The latter were followed until the oscillations were constant for at least 5 cycles.

Checks were made to confirm the persistence of unsteady behaviour: for the cases $R/R_c = 100, 200$, $p = 6{\cdot}8$, $\lambda = \sqrt{2}$ runs were made on meshes with 24×34 and 48×68 intervals and the results agreed to within 2%. Furthermore, the range of variation in N actually increased slightly with higher resolution, as shown in table 3. In general it was found that inadequate vertical resolution suppressed unsteady convection when it was present. On the other hand, when the solutions were converging to a steady state the high resolution cases converged more rapidly than the coarse ones (cf. Schneck & Veronis 1967).

The finite-difference method described above differs slightly from that adopted by Fromm (1964), who calculated all points at each time level, thereby simplifying the solution of Poisson's equation. For the convection calculations he had $N_z \leqslant 26$. Deardorff (1964) used a similar method, with $N_z = 32$; at $R \approx 1000R_c$ he found a Nusselt number of 15, which is 30% lower than the value we predict. Veronis (1966) devised an entirely different approach: he expanded T, ω and ψ in truncated Fourier series and solved a set of coupled nonlinear ordinary differential equations for the Fourier coefficients. For a given number of points the Fourier representation is more accurate (Orszag 1971), though the nonlinear interactions may be more difficult to compute. Veronis's expansion had the form

$$\psi = \sum_m \sum_n a_{mn} \sin(m\pi x/\lambda) \sin n\pi z, \tag{34}$$

summed over positive integral values of m and n such that $m+n \leqslant q$. His published results have $q \leqslant 10$, which enabled him to treat Nusselt numbers up to 7 with errors of less than 1%.

4. Results

4.1. *High Rayleigh number convection in water*

We have systematically investigated the effect of varying the Rayleigh number at a fixed Prandtl number $p = 6{\cdot}8$, corresponding to water at room temperature: Veronis (1966) solved the equations for $R \leqslant 50R_c$; we have repeated his calculations and extended them to $R = 1000R_c$. This has enabled us to identify different regimes of behaviour.

Viscous regime. Linear theory (Chandrasekhar 1961, chap. 2) predicts instability, at $R = R_c = \frac{27}{4}\pi^4 \approx 657{\cdot}5$, to convection in rolls with $\lambda = \sqrt{2}$. Veronis accurately treated cases with this cell width for $R \leqslant 40R_c$. Our investigation for $1{\cdot}1 \leqslant R/R_c \leqslant 40$ was done primarily to confirm the accuracy of the computer program by reproducing his results. Values of the Nusselt number are compared in table 1: each value of R was run on a 24×18 mesh over the half-cell $0 \leqslant x \leqslant \frac{4}{3}$,

		N	
R/R_c	Veronis (1966), $q = 10$	Low resolution, 24×18	High resolution, 48×34
1	1	—	—
1·1	1·18	1·16	—
1·2	1·34	1·32	—
1·4	1·61	1·58	—
2	2·14	2·12	2·14
3	2·68	2·65	—
4	3·04	3·01	—
6	3·55	3·52	—
10	4·24	4·19	—
15	4·85	4·78	—
20	5·33	5·24	5·30 (5·32)
30	6·08	5·97	—
40	6·68	6·56	6·67
50	7·16	7·05	— (7·34)

TABLE 1. Heat flux as a function of Rayleigh number; $p = 6{\cdot}8$, $R \leqslant 50R_c$. Bracketed figures obtained with $\Delta x \neq \Delta z$, see table 2.

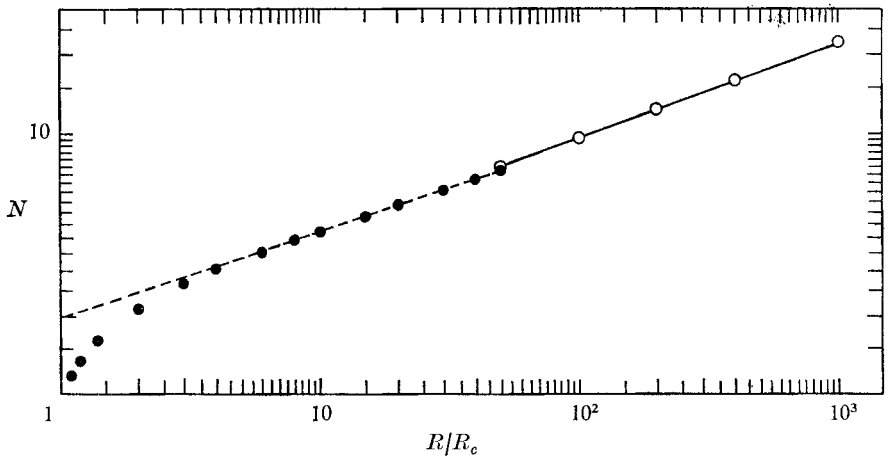

FIGURE 1. Heat flux as a function of Rayleigh number, $p = 6{\cdot}8$. Logarithmic plot of N against R/R_c: – – –, $N = 1{\cdot}96(R/R_c)^{\frac{1}{3}}$; ——, $N = 1{\cdot}8(R/R_c)^{0.365}$; ●, $\lambda = \sqrt{2}$; ○, $\lambda = 1$.

$0 \leqslant z \leqslant 1$; some values were repeated on a 48×34 mesh. In models with $\Delta x = \Delta z$ it was not possible to obtain the exact width $\lambda = \sqrt{2}$. However, this seems of little consequence for low Rayleigh numbers: at $R = 10R_c$ Veronis showed that a 10 % variation in λ produced a variation of only 0·5 % in N.

The agreement between our finite-difference calculations and Veronis's integration in Fourier space is very satisfactory, provided enough points are used, and our results for $R = 20R_c$, $p = 6{\cdot}8$ and $\lambda = \sqrt{2}$ are identical with those in figures 3 and 5 of his paper. Contour plots of T, ω and ψ at $R/R_c = 3$, 5, 7, 10, 15, 18·5 have already been published by Fromm (1965).

The Reynolds number $Re = w/\nu$ remains small throughout this range and convection settles down to a steady state. The variation of N with R is shown in figure 1. At the onset of instability, $R = R_c$ and $N = 1$. In the range $1 < R/R_c < 5$ N rises steeply and then flattens out, with a logarithmic slope decreasing from 2 to an asymptotic value of $\frac{1}{3}$. For $5 \leqslant R/R_c \leqslant 40$ there is a simple one-third power law:

$$N = 1{\cdot}96(R/R_c)^{0{\cdot}333}, \tag{35}$$

with an error of less than 1 % in the exponent. Herring (1963) predicted this behaviour, though his mean field calculations overestimated the flux by one-third. The relation (35) was obtained by Fromm and is also implicit in Veronis's results, though he expressed them in the form

$$[(R/R_c)N - 1] \propto [(R/R_c) - 1]^{1{\cdot}26}. \tag{36}$$

The behaviour of the Nusselt number for steady convection with $R > 50R_c$ will be described below and the distinction between the viscous and advective regimes will be analysed in § 5.

Dependence on cell width: oscillatory convection. At the critical Rayleigh number convection first sets in with $\lambda = \sqrt{2}$. For higher Rayleigh numbers it is frequently asserted that fluid in an infinite layer will choose the horizontal form that maximizes the Nusselt number (Malkus 1954). This hypothesis provides a convenient criterion for adopting a particular cell width in two-dimensional calculations, though Foster (1969) and Ogura (1971) have shown that steady-state solutions are affected by the initial conditions and not determined uniquely by R and p. Nevertheless, we shall assume that the favoured cell width is indicated by a maximum of N.

The variation of N with λ has been determined at $R/R_c = 2$ and 4 (for $p = 0{\cdot}71$) by Ogura (1971), at $R = 10R_c$ by Veronis and at $R = 18{\cdot}5R_c$ (for $p = 1$) by Fromm. The values of λ for which N is a maximum lie in the range $\sqrt{2} > \lambda \geqslant 1{\cdot}25$ and appear to decrease slightly with increasing R. Table 2 shows the effect of varying the cell width at higher Rayleigh numbers. At $R = 50R_c$ there are transient oscillations about a state of steady convection for all $\lambda \leqslant 2$; but the Nusselt number is now a maximum for square cells, with $\lambda = 1$. When $R = 100R_c$ the form of the solutions has changed: steady convection is no longer possible for $\lambda = \sqrt{2}$. Instead there are finite amplitude oscillations, with a variation of 5 % in N. In square cells steady convection still occurs and the heat flux is greater than the average over an oscillation at $\lambda = \sqrt{2}$. This behaviour persists when R is increased, as can be seen from figure 2, where our results are compared with Fromm's and with those obtained by Herring (1963) and Huppert (1973) using the mean field approximation. We shall first examine the oscillatory solutions and then return to steady convection with $\lambda = 1$.

The extreme values of the Nusselt number are listed in table 3. In a series of runs on a 24×34 mesh with $\lambda = \sqrt{2}$, the oscillations persisted as the Rayleigh number was increased to $1000R_c$ (though the actual numerical values are not very meaningful for $R > 400R_c$). The boundary conditions prohibit the lateral sloshing investigated by Deardorff & Willis (1965), and the direction of the flow does not

	N						
R/R_c	$\lambda = 2$	$\lambda = \sqrt{2}$	$\lambda = 1$	$\lambda = \frac{2}{3}$	$\lambda = \frac{1}{2}$	N_x	N_z
20	—	5·32	5·35	—	—	24	34
50	6·74	7·34	7·45	6·61	—	24	34
100	—	(9·5)	9·61	—	—	24	34
200	(9·8)	(11·7)	12·42	11·25	9·75	24	34
			12·35			48	48
400	—	—	16·22	—	—	24	64
			15·90			48	64
1000	—	—	22·16	—	—	48	100

TABLE 2. Heat flux as a function of Rayleigh number; $p = 6{\cdot}8$, $R \geqslant 20R_c$. Bracketed figures are average values for oscillatory convection; the mesh intervals are $\Delta x = \lambda/N_x$, $\Delta z = (2N_z)^{-1}$.

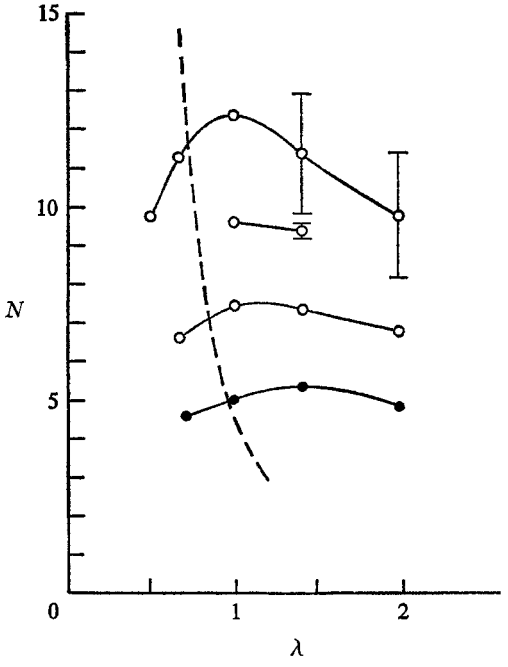

FIGURE 2. Heat flux as a function of cell width, $p = 6{\cdot}8$. Nusselt number plotted against λ for $R/R_c = 18{\cdot}5$, 50, 100, 200. Points show steady solutions; for oscillatory convection the average value of N is shown together with the range of variation. – – –, maximum Nusselt number as predicted by the mean field equations (Huppert 1973); ●—●, Fromm (1965); ○—○, present results.

reverse during an oscillation. The variations correspond to fluctuations in temperature, etc., with a period that is approximately one-third of the circulation time for the cell.

Figure 3 shows a sequence of vorticity profiles, streamlines and isotherms during one oscillation at $R = 200R_c$. The changes in vorticity are striking – the maximum value of $|\omega|$ varies between 0·16 and 0·24 in the course of the oscillation –

	N					
	$\lambda = 2$		$\lambda = \sqrt{2}$			
R/R_c	Min	Max	Min	Max	N_x	N_z
100	—	—	9·28	9·65	24	34
			9·30	9·68	24	68
			9·17	9·56	48	68
150	—	—	10·4	11·5	24	34
200	8·2	11·4	10·5	13·0	24	34
			9·8	12·9	48	68
300	—	—	10·1	14·6	24	34
400	—	—	10·8	16·3	24	34

TABLE 3. Oscillatory convection, $p = 6{\cdot}8$.

but the form of the oscillation appears most clearly from the temperature. Three pairs of hot and cold regions circulate round the cell, affecting the generation and dissipation of vorticity. The approximately sinusoidal behaviour of the velocities and heat fluxes, together with their phase relationships, can be seen from figure 4. Although N varies by only 20 % at $z = 0, 1$, the heat flux at $z = \frac{1}{2}$ changes by an order of magnitude. Outside the boundary layer, heat transport is dominated by rising thermals and their sinking counterparts. The mechanism producing this behaviour will be discussed in § 5.

Advective regime. When $R \geqslant 50R_c$ the heat flux is a maximum for square cells. Values of the Nusselt number calculated with $\lambda = 1$ for $50 \leqslant R/R_t \leqslant 1000$ are given in table 2 and also plotted as a function of the Rayleigh number in figure 1. The one-third law no longer holds over this range; instead, the heat flux follows a power law of the form

$$N = 1{\cdot}8(R/R_c)^{0{\cdot}365}. \tag{37}$$

(The exponent in (37) has an error of less than 1 %; the slope of the curve diminishes slightly towards the highest value of R but this decrease is not significant.) This value of N is greater than that from equation (35) for $R > 15R_c$. At high Rayleigh numbers the favoured cell size is narrower and convection in square cells becomes more efficient than the viscous regime described by (35). Vorticity, instead of being dissipated locally in the vertical plumes, is advected into the thermal boundary layers and lost there.

The detailed structure of the flow for $R = 1000R_c$, the highest Rayleigh number studied, is depicted in figure 5. Comparison of the streamlines and isotherms with those for $R = 20R_c$ shows that the nonlinear features have become even more pronounced. The streamlines are, as always, similar but the thermal boundary layers at $z = 0, 1$ are very narrow, while the rising plume has become attenuated and curves sharply round. The central isothermal region occupies almost all of the cell. The mean temperature gradient for $R = 20R_c$ is stably stratified in this central region (Veronis 1966) but this reversal can no longer be

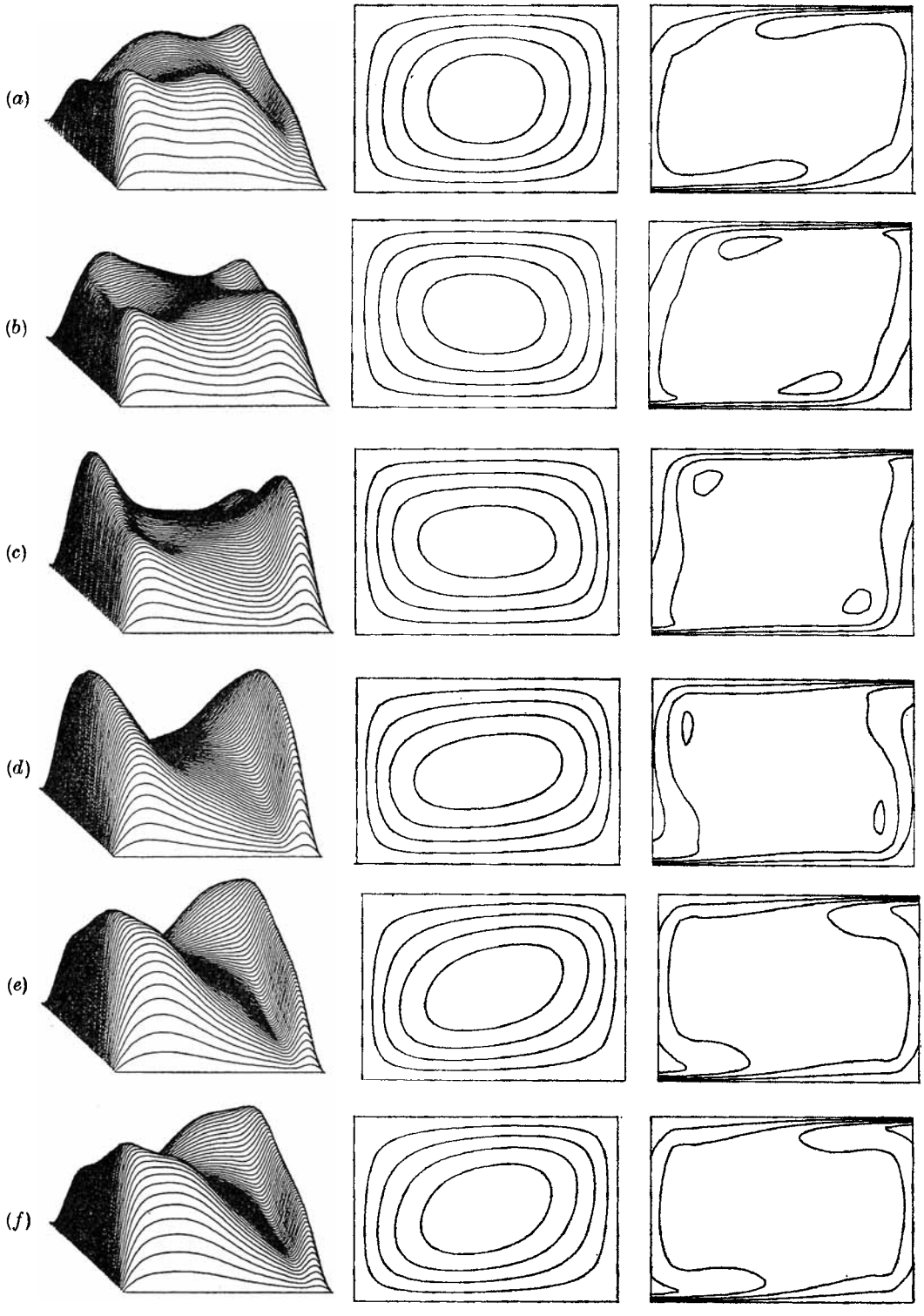

FIGURE 3. Oscillatory convection, $R = 200R_c$, $p = 6{\cdot}8$, $\lambda = \sqrt{2}$. Vorticity profiles, streamlines and isotherms during a single oscillation. The time increment between successive plots is one-sixth of the period.

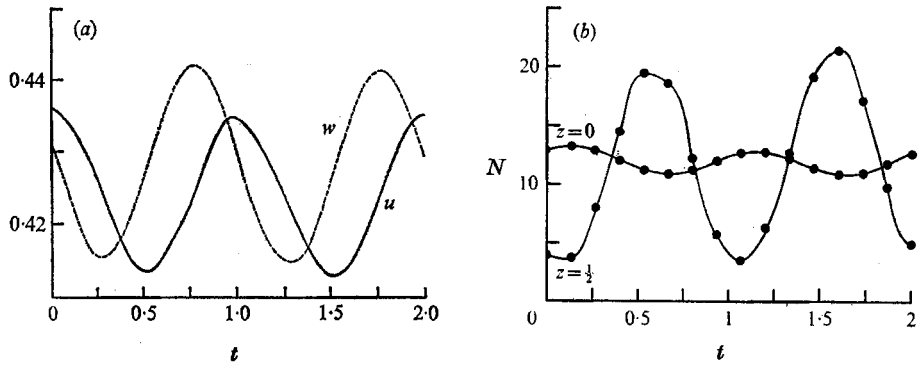

FIGURE 4. Oscillatory convection: variation with time of the velocities and heat flux. (*a*) Maximum values of u and w, the horizontal and vertical velocities. (*b*) Nusselt number N, evaluated at $z = 0$ and $z = \frac{1}{2}$. Times are given in terms of the oscillation period (3·6 dimensionless units).

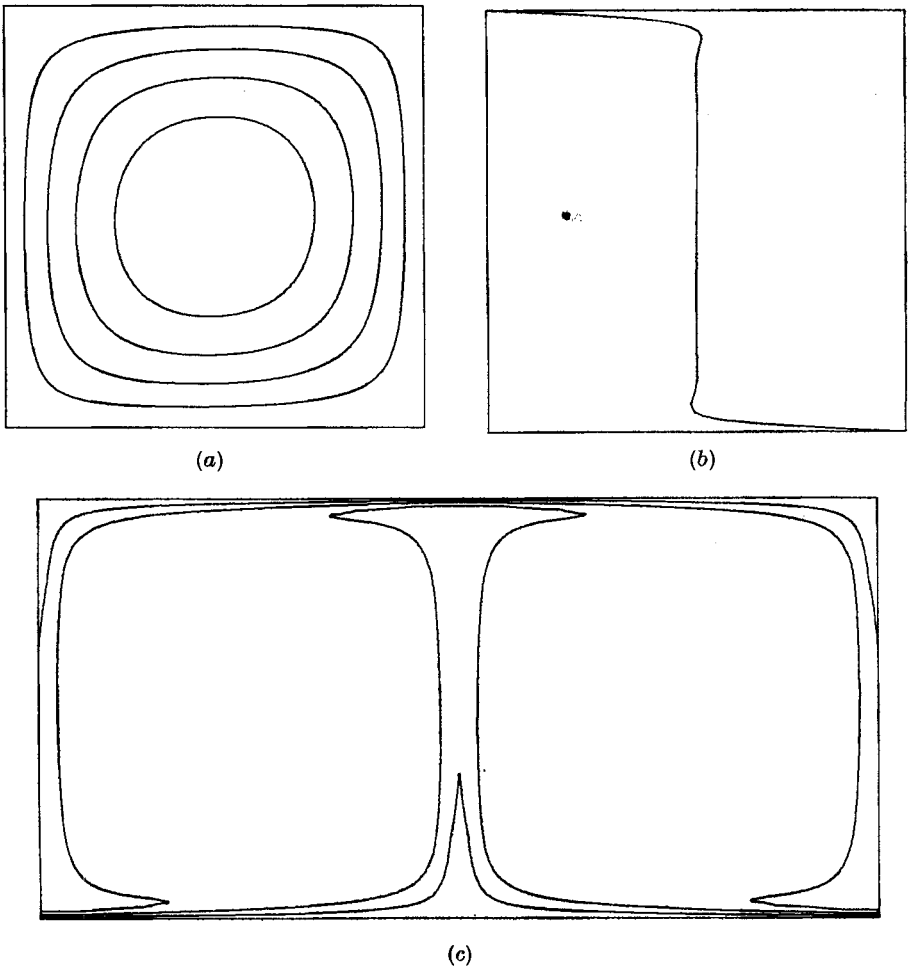

FIGURE 5. Convection in the advective regime, for $R = 1000R_c$, $p = 6{\cdot}8$, $\lambda = 1$. (*a*) Streamlines; (*b*) vertical profile of mean temperature; (*c*) isotherms.

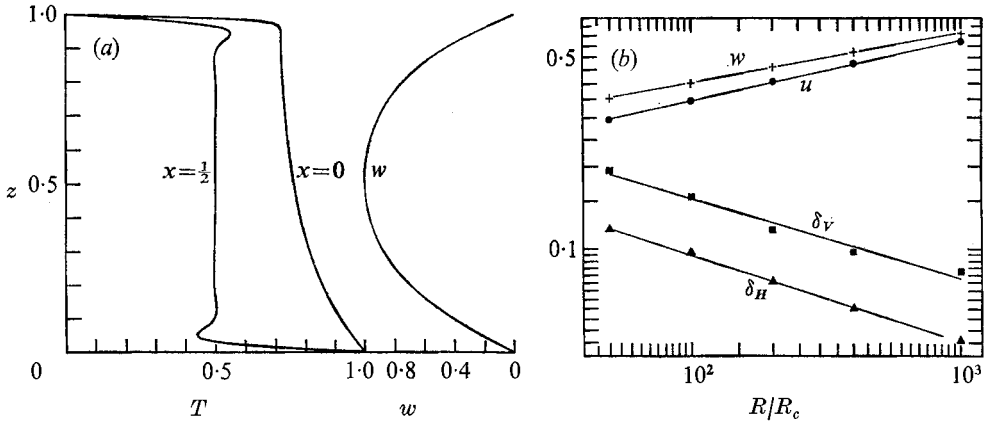

FIGURE 6. (*a*) Vertical profiles for $R = 1000R_c$, $p = 6{\cdot}8$, $\lambda = 1$. Temperature: $T(\frac{1}{2}, z)$ and $T(0, z)$; normalized vertical velocity: $w(0, z)$. (*b*) Advective regime: variation of velocities and boundary-layer thickness with Rayleigh number for $p = 6{\cdot}8$. Logarithmic plots (with slopes shown in brackets) of the thickness of the horizontal boundary layer δ_H ($-0{\cdot}32$), the width of the vertical plume δ_V ($-0{\cdot}29$) and then of the maximum horizontal and vertical velocities (0·22 and 0·18 respectively), as functions of R/R_c.

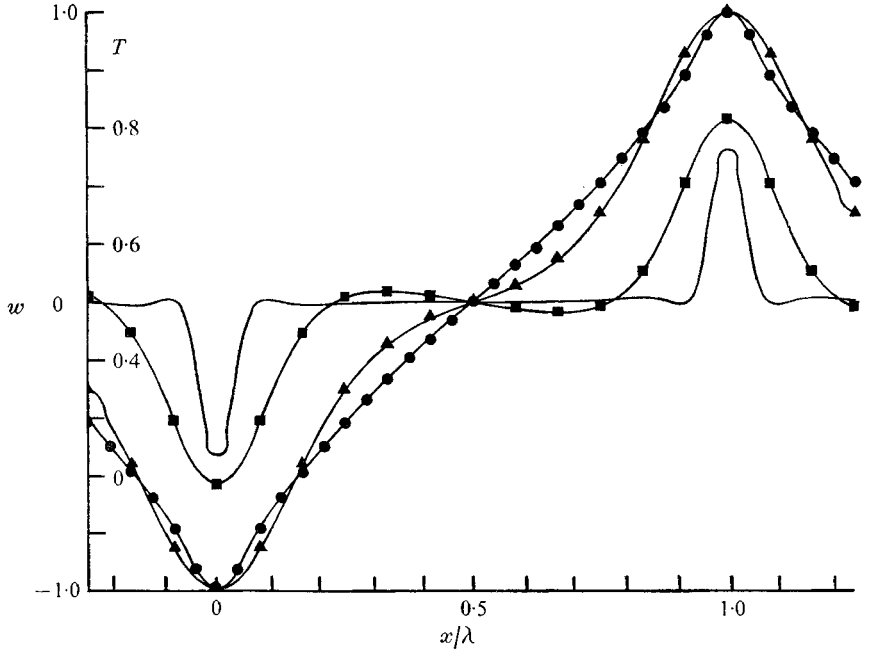

FIGURE 7. Horizontal profiles for $R = 20R_c$ ($\lambda = \sqrt{2}$) and $R = 1000R_c$ ($\lambda = 1$) with $p = 6{\cdot}8$. The temperature $T(x/\lambda, \frac{1}{2})$ and the normalized vertical velocity $w(x/\lambda, \frac{1}{2})$ are plotted as functions of x/λ. T: ——, $R = 1000R_c$; ■—■, $R = 20R_c$. w: ●—●, $R = 1000R_c$; ▲—▲, $R = 20R_c$.

discerned at $R = 1000R_c$. The temperature in the central core is virtually constant, though the kinks in the mean temperature profile just before the boundary layers are real and caused by the plumes spreading out horizontally as they approach the boundaries. This behaviour appears clearly in vertical profiles of T at $x = 0, \frac{1}{2}$, shown in figure 6(*a*). The vertical velocity in the plumes varies approximately sinusoidally with z: acceleration by the buoyancy force is counteracted by an adverse pressure gradient.

Figure 7 shows horizontal profiles of temperature and vertical velocity at $z = \frac{1}{2}$. The vorticity in the isothermal core is nearly constant and the central region therefore rotates with a uniform angular velocity, accelerating slightly in the plumes. This becomes more marked at high Rayleigh numbers and the temperature profiles show that convection of heat is increasingly concentrated into plumes. Although the central core becomes more nearly isothermal there is always a region with a small reversed horizontal temperature gradient between the core and the plumes. This is a consequence of advecting the temperature (cf. the magnetic fields described by Weiss 1966) and causes a local decrease in vorticity.

The variation of the convective velocities and boundary-layer thicknesses with R is plotted in figure 6(*b*). For the horizontal boundary layers the thickness is defined by the points where $T = 0{\cdot}5$; for the plumes it is calculated similarly from $T(x, \frac{1}{2})$. The width of the vertical plumes is then about 1·7 times the thermal-boundary-layer thickness. For the one-third power law of (35) we would expect the boundary-layer thickness δ, the dimensionless velocity $|\mathbf{u}|$ and the kinetic energy density $\mathscr{E}$ to vary as powers of R:

$$\delta \propto R^{-\frac{1}{3}}, \quad |\mathbf{u}| \propto R^{\frac{1}{3}}, \quad \mathscr{E} \propto R^{\frac{1}{3}} \tag{38}$$

(see § 5). The actual thicknesses of boundary layers and plumes are consistent with (38) but the r.m.s. velocity increases more rapidly, as $R^{0{\cdot}18}$. Thus the enhanced heat flux of equation (37) is apparently achieved by increasing the velocity without significantly changing the temperature field.

4.2. *Effect of varying the Prandtl number*

Variation of heat flux. Veronis calculated the Nusselt number $N(R, p, \lambda)$ for models with $\lambda = \sqrt{2}$, $100 \geqslant p \geqslant 0{\cdot}005$ and $R \leqslant 20R_c$. We have computed heat fluxes for $\lambda = 1$, $p \geqslant 0{\cdot}01$ and $R \leqslant 1000R_c$. These results are shown in table 4: values of N are accurate to within 1 % except for runs with $R = 1000R_c$, where the error may be as high as 2·5 %. Models with infinite Prandtl number required a modified version of the program, developed for geophysical problems (McKenzie, Roberts & Weiss 1973). The Nusselt numbers for $p = \infty$ agree with those computed by Straus (1972) for $R \leqslant 60R_c$ and are consistent with an asymptotic dependence of the form $N = 2{\cdot}00(R/R_c)^{\frac{1}{3}}$. We have also recomputed $N(20R_c, 0{\cdot}01, \sqrt{2})$ for comparison with Veronis's result and they agree to within 1 %. The variation of N with λ is somewhat greater for the advective than for the viscous regime.

Veronis observed that the values in table 4 show a definite pattern. For $p < 1$ the heat flux is independent of the Prandtl number; as p increases the Nusselt

	p						
R/R_c	0·01	0·1	1·0	6·8	16	100	∞
6	3·61	3·61	3·58	3·55	3·54	3·55	3·55
10	4·39	4·39	4·38	4·24	4·22	4·24	4·24
15	5·11	5·11	5·06	4·85	4·82	4·85	4·83
20	5·68	5·67	5·62	5·33	5·29	5·33	5·29
	5·62	**5·62**	**5·53**	**5·35**	**5·35**	**5·36**	**5·37**
50	**7·91**	**7·92**	**7·81**	**7·45**	**7·31**	**7·30**	**7·32**
100	—	**10·18**	**10·09**	**9·61**	**9·32**	—	**9·25**
200	—	**13·01**	**12·93**	**12·35**	**11·84**	—	**11·52**
400	—	—	**16·55**	**15·90**	—	—	**14·45**
1000	—	—	**22·93**	**22·16**	—	—	**19·47**

TABLE 4. Nusselt number as a function of R and p. Values in bold-face for $\lambda = 1$. Other values for $\lambda = \sqrt{2}$ (results for $p = 0{\cdot}01$, $0{\cdot}1$, $1{\cdot}0$, $6{\cdot}8$, 100 from Veronis 1966).

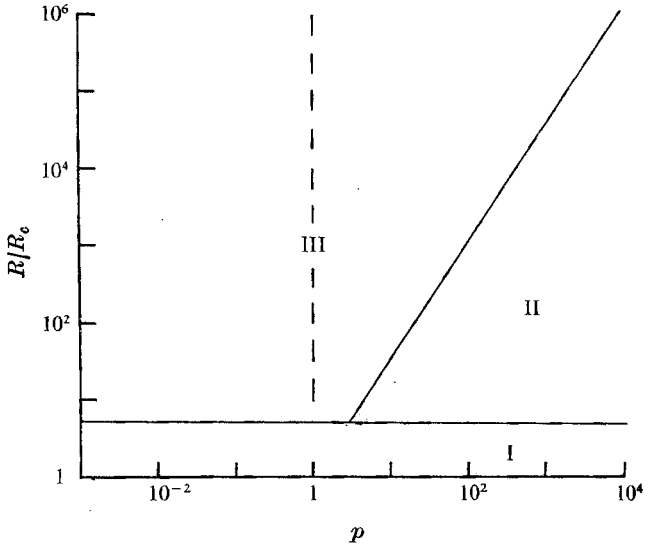

FIGURE 8. Regimes of convection in the R, p plane. I, low Rayleigh number convection; II, viscous regime; III, advective regime; the dashed line separates high and low Prandtl number behaviour.

number declines slightly between $p = 1$ and $p = 6{\cdot}8$. Thereafter, the heat flux is once again independent of p for Rayleigh numbers less than $20R_c$. The variation of N with R provides more information: for $p = 0{\cdot}1$ and $p = 1$ we find that $N \propto R^{0{\cdot}362}$ over the range $20 \leqslant R/R_c \leqslant 200$; while, from Veronis's results, $d\ln N/d\ln R \approx 0{\cdot}365$ when $R \sim 20R_c$ and $p \leqslant 0{\cdot}025$. Thus convection at low Prandtl numbers shows the same power-law dependence as we found for the advective regime at $p = 6{\cdot}8$.

We can summarize this behaviour in terms of a general power law

$$N = A(p)\,(R/R_c)^{\beta}. \tag{39}$$

The R, p plane can be divided into three regions (figure 8). In region I the Nusselt number rises steeply from unity at $R = R_c$ and the heat flux can be calculated

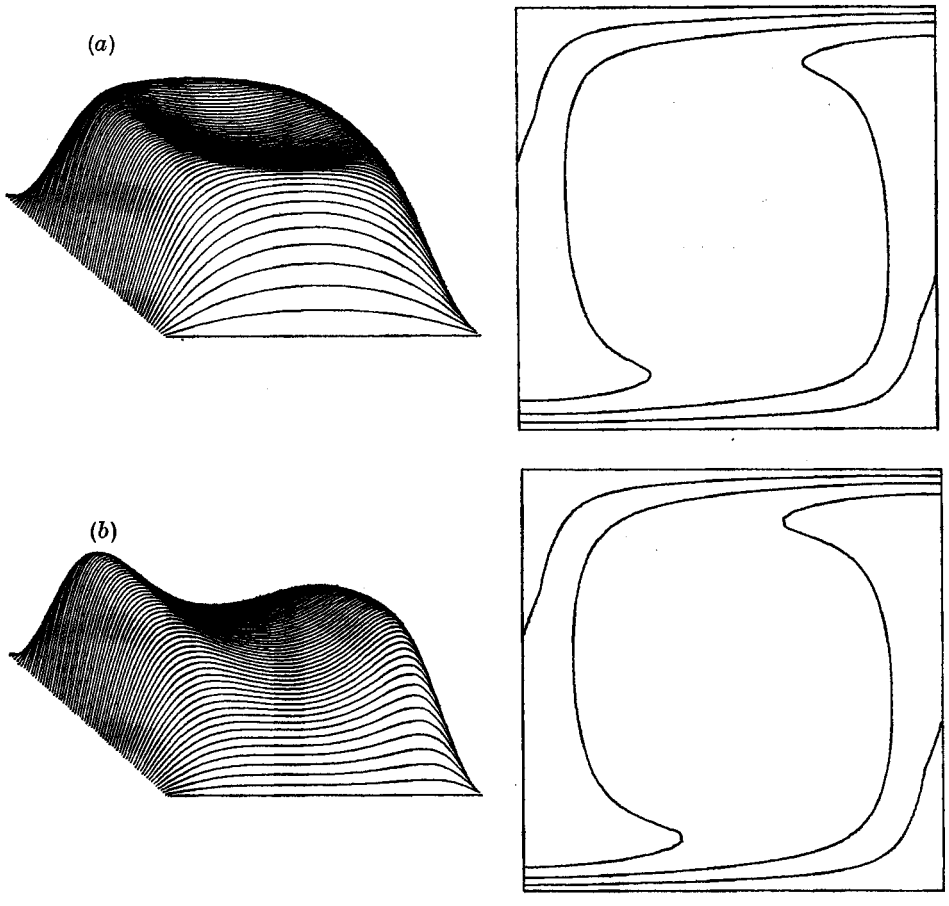

FIGURE 9. The effect of varying Prandtl number, with $R = 50R_c$, $\lambda = 1$. Vorticity profiles and isotherms (*a*) for $p = 0{\cdot}01$, (*b*) for $p = 100$.

by high-order expansion methods (Malkus & Veronis 1958; Kuo 1961). Region II is the viscous regime discussed above, with N given by (35) so that

$$\beta = 0{\cdot}333 \pm 0{\cdot}002$$

and A is independent of p in (39). This region only exists for Prandtl numbers greater than unity. Region III is the advective regime. Here $\beta = 0{\cdot}365 \pm 0{\cdot}003$ and A is a slowly decreasing function of p: $A(16) = 1{\cdot}7$, $A(6{\cdot}8) = 1{\cdot}8$ and $A(p) \to 1{\cdot}90$ as $p \to 0$. As the Prandtl number increases, the efficiency of this advective regime is impaired and the viscous regime extends to higher Rayleigh numbers. Ultimately, when p is infinite, the advective term in (10) vanishes for all finite R. The boundary between regions II and III is poorly determined from our data; for $p = 6{\cdot}8$, 16 it is given by $R/R_c \approx p^{1{\cdot}5 \pm 0{\cdot}3}$. This is consistent with the expression

$$R/R_c = (1{\cdot}1 \pm 0{\cdot}1)p^{\frac{3}{2}}. \tag{40}$$

From (35), (37) and (40) it follows that $A(p) \approx 1{\cdot}95p^{-0{\cdot}05}$ for $p \geqslant 6{\cdot}8$.

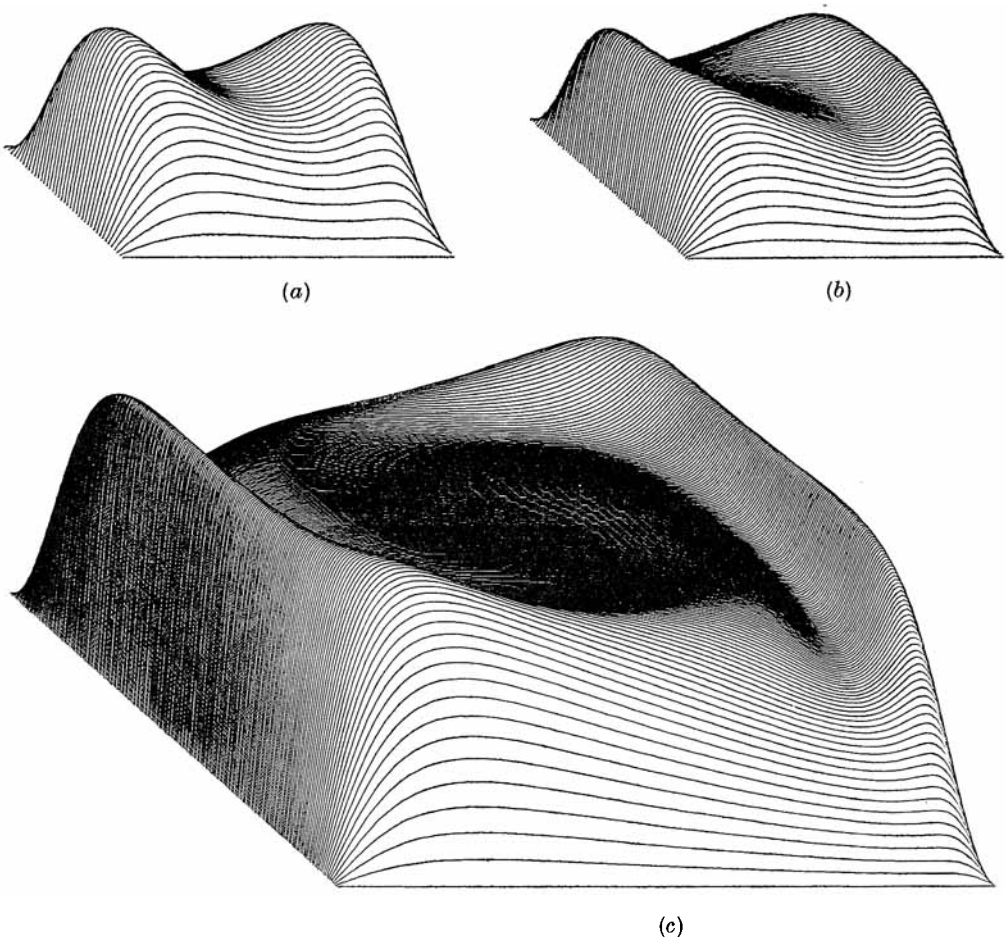

FIGURE 10. The dependence of the vorticity on the Rayleigh number, for $p = 6{\cdot}8$. Vorticity profiles: (*a*) for $R = 20R_c$, $\lambda = \sqrt{2}$, (*b*) for $R = 100R_c$, $\lambda = 1$ and (*c*) for $R = 1000R_c$, $\lambda = 1$.

General behaviour. For a fixed value of R the Nusselt number changes by only 7 % when p is altered by 10^4. Figure 9 shows the isotherms for $R = 50R_c$ with $p = 0{\cdot}01$ and $p = 100$. They too are scarcely affected, though the velocities vary in order to maintain a constant flux and the dimensionless kinetic energy density $\mathscr{E}$ is inversely proportional to p.

The vorticity shows more striking differences and provides the best means of distinguishing the different regimes. Its behaviour at low Rayleigh numbers is shown in figure 5 of Fromm's paper; for $R < 5R_c$ the vorticity resembles the linear solution with $\omega \propto \sin \pi x/\lambda \sin \pi z$. Profiles for $p = 6{\cdot}8$ with $R/R_c = 20$, 100 and 1000 are plotted in figure 10. When $R = 20R_c$ the central peak has separated into two humps, centred on the regions with horizontal temperature gradients, where vorticity is generated. In the viscous regime advection is unimportant and vorticity is dissipated where it is created, in the plumes. As R is increased, vorticity is carried towards the horizontal boundaries and dissipated by viscosity

near the corners of the cell, while ω scarcely varies in the central core; this behaviour characterizes the advective regime.

The effect of changing the Prandtl number is shown by the vorticity profiles for a fixed Rayleigh number, $R = 50R_c$, at $p = 0{\cdot}01$ and $p = 100$, plotted in figure 9. For $p = 100$, the vorticity is concentrated on the sides of the thermal plumes and ω is approximately harmonic in the centre, with a saddle-point at $x = z = \frac{1}{2}$. When $p = 0{\cdot}01$, vorticity is advected round, producing a band of high vorticity with a flattish minimum in the centre, and the angular velocity increases to a maximum at the edges of the plumes. Thus convection at high and low Prandtl numbers is distinguished by different distributions of vorticity.

5. Physical interpretation

5.1. *Steady convection*

The simplest behaviour occurs for the viscous regime in region II of figure 8, where $N \propto R^{\frac{1}{3}}$. This viscous regime can easily be understood in terms of a simple boundary-layer model (Turcotte & Oxburgh 1967; Robinson 1967). We shall henceforth revert to physical (dimensional) units. Consider a roll with width $L \sim d$. Let ω be the vorticity and w the velocity in the plumes; then at the perimeter of the isothermal core

$$w \sim \omega d. \tag{41}$$

In the horizontal boundary layers,

$$u\,\partial T/\partial x \sim \kappa\,\partial^2 T/\partial z^2, \tag{42}$$

whence

$$w \sim \left(\frac{d}{\delta}\right)^2 \frac{\kappa}{d}, \tag{43}$$

if we assume that $u \sim w$ and thus that horizontal boundary layers and vertical plumes have the same thickness δ. In the plumes, vorticity is created and dissipated locally, so that

$$\nu\nabla^2\omega \sim g\alpha\,\partial T/\partial x \tag{44}$$

or, from (41),

$$w \sim \frac{g\alpha\Delta T d^2}{\nu}\left(\frac{\delta}{d}\right). \tag{45}$$

Then, from (17), (43) and (45),

$$(\delta/d) \sim R^{-\frac{1}{3}}, \quad w \sim R^{\frac{2}{3}}\kappa/d, \tag{46}$$

while the Nusselt number

$$N \sim (d/\delta) \propto R^{\frac{1}{3}}. \tag{47}$$

These predictions are consistent with the numerical results summarized in (38), if the units are transformed according to equation (19). The overall Reynolds number

$$Re = wd/\nu \propto p^{-1}R^{\frac{2}{3}} \tag{48}$$

and so the transition from viscous to nonlinear flow occurs at a Rayleigh number $R \propto p^{\frac{3}{2}}$. Equation (40) shows that this is consistent with the numerical results and the one-third law applies only for $Re \lesssim 10$. Hence the vorticity in the core is approximately harmonic and the steady 'inviscid' solution with ω constant in the central region (Batchelor 1956; Robinson 1967) is not attained in this regime.

When advection of vorticity becomes important vorticity is dissipated around the stagnation points where the plumes impinge on the boundaries. It is no longer feasible to construct a simple model but region III of figure 8 can still be subdivided into two regimes. At large Prandtl numbers an element of fluid gains vorticity as it rises or falls but then loses what was gained through friction as it traverses the thermal boundary layers. Thus the flow is essentially composed of rising and sinking plumes. The vorticity ω_c in the central core is approximately constant and

$$\omega_c \lesssim \omega_0 = \frac{1}{2}\left(\frac{g\alpha\Delta T}{\delta}\right)\frac{d}{w}. \tag{49}$$

The advective regime for $p \ll 1$ is different (Veronis 1966). Viscosity is too feeble for the fluid to lose more than a small fraction of its vorticity as it passes along the horizontal boundaries. So the fluid gains vorticity as it circulates round the cell and this process continues until the total vorticity is so great that viscous losses can balance what is gained. This value of ω is much greater than ω_0, the vorticity gained in one passage through a plume: for example, with $p = 0{\cdot}01$ and $R = 50R_c$, the central vorticity is 9000 times the value given by (49). Convection is no longer dominated by the plumes: instead the flow resembles an inertial flywheel driven by a fixed torque, with friction proportional to its angular velocity. In the isothermal core the Reynolds number is high and so the vorticity is virtually constant in a steady state (Batchelor 1956). This configuration is only slowly achieved and the Nusselt number creeps exponentially to its final value at a rate determined by the viscous time scale for the central core. Since the sign of $\partial T/\partial x$ reverses between the plumes and the central core, as shown in figure 7, ω diminishes before settling down to a constant value. For $p = 0{\cdot}01$ and $R = 50R_c$, ω falls by 14 % of its maximum value and the profiles in figure 10 outline a circular volcano. At much higher Rayleigh numbers we would expect an elevated racetrack enclosing a flat interior basin.

Oscillations. In the advective regime for Prandtl numbers greater than unity there are periodic variations in all quantities. For square cells these fluctuations slowly decay as the convection converges to a steady state. Finite amplitude oscillations persist in wider cells. A linearized analysis might show that steady convection is either stable to small perturbations (so the oscillatory modes are damped) or unstable (so that oscillations grow until they are limited by nonlinear effects), depending on the width. We shall attempt to describe the mechanism that maintains the steady oscillations. The same phenomena appear in a simple model put forward by Welander (1967).

The oscillations themselves are thermal in origin. Suppose that an abnormally cold parcel of fluid falls from the upper surface: then it will remain colder as it circulates round the cell. On a fixed Eulerian mesh there will be variations of temperature, repeated each time the cold blob passes by. This behaviour is visible in the isotherms of figure 3. The cold plume bulges and the hot rising plume is pinched off as colder fluid enters it. At the same time, symmetry requires a parcel of hotter fluid, following the cold fluid around, and in general we might find m such pairs. The symmetry assumed for high resolution runs allows only

modes with m odd. However, no even modes were found in models computed for a full half-cell ($0 \leqslant x \leqslant L$, $0 < z < d$).

Thermal diffusion normally eliminates these fluctuations: for example, at $R/R_c = 400$ and 1000 with $\lambda = 1$ the oscillations showed periodicities corresponding to $m = 1$ and to $m = 3$ which decayed exponentially on the thermal time scale. The oscillations are maintained only if the velocity is coupled to the thermal field, so that cold fluid moves rapidly past the lower (hot) boundary and slowly past the upper one (Welander 1967). This coupling can just be detected in the streamlines of figure 3 and it is clearly seen in the vorticity profiles. Now vorticity generated by horizontal temperature gradients in the plumes is advected into the horizontal boundary layers. The vorticity near the boundaries depends also on local temperature gradients and viscous dissipation. Colder fluid reaches the lower boundary with more vorticity and therefore travels faster, losing less heat as it goes across. As this fluid crosses the cell the horizontal temperature gradient steepens and vorticity continues to be created, reducing the effect of viscous losses. Behind the cold blob, however, the isotherms are drawn out and friction retards the flow until the temperature rises and isotherms reconnect. There is thus an adverse temperature gradient which further reduces the speed. Conduction of heat from the boundary then causes the formation of a hot spot. This follows at a distance of about $\frac{1}{2}L$ behind the cold region, corresponding to an oscillation with $m = 3$, the only mode found in the numerical experiments.

This process requires that vorticity be advected into the boundary layer, where viscous diffusion must be significant. For $p < 1$ the overall vorticity cannot be altered sufficiently in an oscillation, so large Rayleigh and Prandtl numbers are necessary for oscillations to occur. Increasing the cell width enhances the effect of viscosity, as can be seen by comparing the vorticities in figure 10. Eddies with $\lambda \gg 1$ might be expected to split in three. However, we have found no indication of fission for cells with $R = 200R_c$, $\lambda \leqslant 4$. The behaviour of an infinite layer is not obvious from our numerical experiments on a single cell. It is probable that infinitesimal perturbations would develop into steady convection, though suitable initial conditions would allow oscillatory solutions to persist. Once some pattern of cellular convection is established, the total number of cells can change only by the consumption of small cells or the fission of larger ones, while the cell widths grow more uniform on a time scale that is determined by diffusion.

6. Conclusion

These numerical experiments have enlarged our physical understanding of two-dimensional convection between free boundaries and it is not obvious that extensions to higher Rayleigh numbers, or to smaller Prandtl numbers, will introduce any new phenomena. Some points still need to be clarified. The transition to the advective regime – the curve separating regions II and III of figure 8 – might be more precisely determined. The exponent, $\beta = 0{\cdot}365$, in (37) appears to be constant over the range $50 \leqslant R/R_c \leqslant 1000$, but much greater values of R would have to be investigated in order to determine whether the heat flux has the form

$$N \propto R^{\frac{1}{3}}[\ln (R/R_0)]^{\gamma}, \tag{50}$$

where γ and R_0 are constants of order unity. Similarly, we could find no evidence that the favoured cell width changes for $R > 50R_c$, though it might decrease with increasing p.

Our results provide the first clear evidence for a power law with an exponent greater than $\frac{1}{3}$. Howard (1963) used integrals of (3) and (7) to obtain an upper bound of $\frac{1}{2}$ for the exponent in the limit of large R. For a single horizontal mode satisfying (4) and the same integral constraints, the exponent is reduced to $\frac{3}{8}$ (Howard 1963; Straus 1973); this provides an upper bound for all mean field and single mode calculations. It is interesting that the value obtained from numerical experiments lies between $\frac{1}{3}$ and $\frac{3}{8}$. However, when many modes are allowed (corresponding to fine structure in thermal boundary layers and the vertical plumes) the upper bound has an exponent of $\frac{1}{2}$ for $R \gg 1$ (Busse 1969). The computed value of 0·365 lies well below this limit.

Gough, Spiegel & Toomre (1973) have recently studied three-dimensional convection between free and fixed boundaries, obtaining asymptotic results for a cellular model together with numerical solutions of the modal equations up to $R = 10^{25}$. For two-dimensional rolls their model is identical to Herring's; for three-dimensional motion with free boundaries they find that $N \propto R^{\frac{1}{3}}$ when p is infinite but that $N \propto [R \ln R]^{\frac{1}{5}}$ when p is of order unity. Numerical experiments confirm their prediction that for high Prandtl number the $R^{\frac{1}{3}}$ law holds at much lower Rayleigh numbers for free than for fixed boundaries.

Two-dimensional rolls are found in convection experiments at low Rayleigh numbers, but it is doubtful whether our results are relevant to convection between fixed boundaries, where the thermal boundary layer itself becomes unstable. Busse (1967) showed that when $p \gg 1$ rolls become unstable to three-dimensional disturbances for $R \gtrsim 13R_c$ and the resulting bimodal convection has been investigated experimentally by Busse & Whitehead (1971). Although convection becomes time-dependent at higher Rayleigh numbers, or when $p < 1$ (Rossby 1969), it is uncertain whether the oscillations correspond to circulating hot and cold spots (Krishnamurti 1970) or to displacements of the cells (Willis & Deardorff 1970).

The onset of convection between free boundaries has been studied in the laboratory (Goldstein & Graham 1969) but there is no experimental evidence on the persistence of two-dimensional rolls. The thermal boundary layers remain stable if $d \ln N / d \ln R \geqslant \frac{1}{3}$ (Busse 1967) and Straus (1972) has confirmed, for $p \gg 1$, that rolls are stable to the three-dimensional perturbations that lead to bimodal convection. The viscous regime described above should therefore be a stable solution to the full three-dimensional problem. At low Prandtl numbers, however, rolls are unstable to oscillatory three-dimensional disturbances which generate vertical vorticity and so produce wavelike distortions of the rolls (Busse 1972). These probably correspond to the oscillations found in experiments with fixed boundaries. Thus it seems likely that the two-dimensional advective regime described here will become unstable to wavelike disturbances and that these will eventually lead to fully three-dimensional cellular convection.

Convection between fixed plates is dominated by viscous boundary layers but stress-free boundaries are more appropriate in astrophysics. Apart from its

intrinsic interest, the idealized model that we have studied is a necessary preliminary to more complicated problems, such as penetrative convection and the effects of magnetic fields or compressibility. In stars the radiative conductivity is high and the effective Prandtl number is small. It has been conjectured that the heat flux should be independent of both ν and d, so that

$$N \propto (pR)^{\frac{1}{3}}. \tag{51}$$

In calculating models of convective stellar atmospheres the depth d is replaced by a mixing length; it is generally assumed that fluid loses its kinetic energy after rising through a mixing length, so that

$$N \propto (pR)^{\frac{1}{2}} \tag{52}$$

for $pR \gg 1$ and the heat flux is independent of both κ and ν (Spiegel 1971*a*, *b*). Our two-dimensional models with pR of order unity show no such variation of N with p. Stellar convection requires a study of three-dimensional models at low Prandtl numbers, with $pR \gtrsim 10^3$.

We wish to thank Dr D. O. Gough for many discussions which have improved our understanding of convection. The program was developed in collaboration with Dr R. S. Peckover and most of the computing was done on the IBM 360/44 at the Institute of Theoretical Astronomy; we are grateful to Mr N. J. Butler for his co-operation and assistance in producing the diagrams. Further computations were carried out at the Max-Planck-Institut für Astrophysik, Munich, and we are grateful to Dr K. von Sengbusch for his assistance and advice. This paper was written mainly at the Max-Planck-Institut für Astrophysik and improved as a result of comments by Dr F. H. Busse, Dr Gough and Dr H. E. Huppert. D. R. M. is grateful to I.B.M. (United Kingdom) Ltd. for a graduate fellowship held while this research was being done.

REFERENCES

Batchelor, G. K. 1956 *J. Fluid Mech.* **1**, 177.

Brindley, J. 1967 *J. Inst. Math. Applics.* **3**, 313.

Busse, F. H. 1967 *J. Math. & Phys.* **46**, 140.

Busse, F. H. 1969 *J. Fluid Mech.* **37**, 457.

Busse, F. H. 1972 *J. Fluid Mech.* **52**, 97.

Busse, F. H. & Whitehead, J. A. 1971 *J. Fluid Mech.* **47**, 305.

Chandrasekhar, S. 1961 *Hydrodynamic and Hydromagnetic Stability.* Clarendon Press.

Deardorff, J. W. 1964 *J. Atmos. Sci.* **21**, 419.

Deardorff, J. W. & Willis, G. E. 1965 *J. Fluid Mech.* **23**, 337.

Foster, T. D. 1969 *J. Fluid Mech.* **37**, 81.

Fromm, J. E. 1964 *Methods in Comp. Phys.* **3**, 346.

Fromm, J. E. 1965 *Phys. Fluids*, **8**, 1757.

Goldstein, R. J. & Graham, D. J. 1969 *Phys. Fluids*, **12**, 1133.

Gough, D. O., Spiegel, E. A. & Toomre, J. 1973 Model equations for turbulent convection. To be published.

Herring, J. R. 1963 *J. Atmos. Sci.* **30**, 325.

HOWARD, L. N. 1963 *J. Fluid Mech.* **17**, 405.

HUPPERT, H. 1973 The asymptotic solution of the mean field equations of thermal convection. In preparation.

KRISHNAMURTI, R. 1970 *J. Fluid Mech.* **42**, 309.

KUO, H. L. 1961 *J. Fluid Mech.* **10**, 611.

MCKENZIE, D. P., ROBERTS, J. M. & WEISS, N. O. 1973 Numerical experiments on convection in the earth's mantle. In preparation.

MALKUS, W. V. R. 1954 *Proc. Roy. Soc.* A **225**, 185.

MALKUS, W. V. R. & VERONIS, G. 1958 *J. Fluid Mech.* **4**, 225.

MOORE, D. R., PECKOVER, R. S. & WEISS, N. O. 1973 Difference methods for time-dependent two-dimensional convection. In preparation.

OGURA, Y. 1971 *J. Atmos. Sci.* **28**, 709.

ORSZAG, S. 1971 *J. Fluid Mech.* **49**, 75.

RAYLEIGH, LORD 1916 *Phil. Mag.* **32**, 529.

ROBERTS, K. V. & WEISS, N. O. 1966 *Math. Comp.* **20**, 272.

ROBINSON, J. L. 1967 *J. Fluid Mech.* **30**, 577.

ROSSBY, H. T. 1969 *J. Fluid Mech.* **36**, 309.

SCHNECK, P. & VERONIS, G. 1967 *Phys. Fluids*, **10**, 927.

SPIEGEL, E. A. 1967 In *Aerodynamic Phenomena in Stellar Atmospheres* (ed. R. N. Thomas), p. 348. Academic.

SPIEGEL, E. A. 1971*a* *Comm. Astrophys. & Space Phys.* **3**, 53.

SPIEGEL, E. A. 1971*b* *Ann. Rev. Astro. Astrophys.* **9**, 323.

STRAUS, J. M. 1972 *J. Fluid Mech.* **56**, 353.

STRAUS, J. M. 1973 In preparation.

TURCOTTE, D. L. & OXBURGH, E. R. 1967 *J. Fluid Mech.* **28**, 29.

VERONIS, G. 1966 *J. Fluid Mech.* **26**, 49.

WEISS, N. O. 1966 *Proc. Roy. Soc.* A **293**, 310.

WELANDER, P. 1967 *J. Fluid Mech.* **29**, 17.

WILLIS, G. E. & DEARDORFF, J. W. 1970 *J. Fluid Mech.* **44**, 661.